INRIA

INSTITUT NATIONAL DE RECHERCHE EN INFORMATIQUE ET EN AUTOMATIQUE

An implicit method for turbulent boundary layers simulation

Bruno KOOBUS

N° 2450

Décembre 1994

PROGRAMME 6

ISSN 0249-6399

INRIA
SOPHIA ANTIPOLIS

An implicit method for turbulent boundary layers simulation

Bruno KOOBUS *

Programme 6 — Calcul scientifique, modélisation et logiciel numérique
Projet Sinus

Rapport de recherche n°2450 — Décembre 1994 — 38 pages

Abstract: Here, we describe a numerical method which combines a mixed finite volume/finite element formulation on unstructured triangulations and a linearized implicit method for time advancing. A particular attention has been paid to the source term implicitation.
This method is applied to three typical low-Reynolds number $k-\varepsilon$ models, namely those of Lam-Bremhorst, Nagano-Tagawa and Speziale-Abid-Anderson. The selected test cases consist of a subsonic flow in a duct and a supersonic flow over a flat plate.

Key-words: $k-\varepsilon$ models, low-Reynolds number models, finite element, finite volume, implicit method

(Résumé : tsvp)

*INRIA Sophia Antipolis,B.P. 93, 06902 Sophia-Antipolis Cedex,France

Unité de recherche INRIA Sophia-Antipolis
2004 route des Lucioles, BP 93, 06902 SOPHIA-ANTIPOLIS Cedex (France)
Téléphone : (33) 93 65 77 77 – Télécopie : (33) 93 65 77 65

Une méthode implicite pour la simulation des couches limites turbulentes

Résumé : On propose une méthode numérique qui combine une formulation mixte volumes finis/éléments finis sur des triangulations non structurées et une méthode implicite linéarisée pour l'avancement en temps. Le traitement implicite du terme source a fait l'objet d'une attention particulière.
Cette méthode est appliquée à trois modèles $k - \varepsilon$ bas-Reynolds, à savoir les modèles de Lam-Bremhorst, Nagano-Tagawa et Speziale-Abid-Anderson.
Les cas tests présentés sont un écoulement subsonique de conduite et un écoulement de plaque plane à grand nombre de Mach.

Mots-clé : $k - \varepsilon$, modèles bas-Reynolds, Eléments Finis, Volumes Finis, méthodes implicites

Contents

NOMENCLATURE

Symbol	Description
ρ	fluid density
u	horizontal component of the velocity
v	vertical component of the velocity
E	total energy per unit volume
k	kinetic energy of turbulence
ε	turbulent dissipation rate
p	pressure
T	temperature
x	streamwise coordinate
y	normal distance to the wall
T_w	temperature at the wall
M	Mach number
μ	laminar viscosity
μ_t	eddy viscosity
λ	laminar thermal conductivity
λ_t	eddy thermal conductivity
$\nu = \dfrac{\mu}{\rho}$	kinetic laminar viscosity
$\mathcal{P}$	eddy production term
τ	laminar stress tensor
τ_t	turbulent stress tensor
τ_w	shear stress at the wall
$u_f = \sqrt{\dfrac{\tau_w}{\rho}}$	friction velocity
$y^+ = \dfrac{u_f\ y}{\nu}$	non-dimensional y

$u^+ = \frac{u}{u_f}$	non-dimensional u
$k^+ = \frac{k}{{u_f}^2}$	non-dimensional k
$\varepsilon^+ = \frac{\varepsilon\ \nu}{{u_f}^4}$	non-dimensional ε
$R_t = \frac{\rho k^2}{\mu\varepsilon}$	local Reynolds number
$R_y = \frac{\rho\sqrt{k}y}{\mu}$	local Reynolds number
C_p	specific heat at constant pressure
C_v	specific heat at constant volume
$\gamma = \frac{C_p}{C_v}$	specific heat ratio
n	normal to the wall
subscript e	freestream value
$C_f = \frac{2\tau_\omega}{\rho_e u_e^2}$	wall friction coefficient

Introduction

There is an increasing need to simulate more and more complex turbulent flows using statistical modelling. For such flow calculations, a good compromise between zero or one-equation models and second order closures are the two-equation turbulence models. In particular high-Reynolds number $k-\varepsilon$ models [3] are still widely used in a variety of practical engineering calculations. In these standard models, which are considered valid in the turbulent region (far-wall zones), the near-wall effects are simulated by wall functions which yield boundary conditions for points situated in the turbulent zone. Unfortunately, this procedure is not well adapted for most complex flows of industrial applications such as those involving separation. In such cases, the equations of the model and the boundary conditions (wall functions) may give wrong results.

For that reason, extended $k-\varepsilon$ models (also called low-Reynolds number $k-\varepsilon$ models) which are applicable to the entire domain made of the near-wall zone (low-Reynolds number) and the far-wall zone (high-Reynolds number), have been developed (see [9] for a review) which allow a better treatment of complicated turbulent flows. However these models are often very difficult to integrate numerically, exhibiting unstable numerical behavior very close to the wall. Moreover, simulating complex turbulent flows with such models can be very expensive. Indeed, these turbulence models are integrated directly to the solid boundary and very refined meshes are then required to capture well the near-wall stiff gradients of the turbulence variables.

In such flow calculations, the two main numerical problems concern the approximation on the one hand, and the resolution on the other hand.

Concerning the approximation, when a steady stationary solution is reached, the validity of this solution is not sure. For the most difficult cases, a spatial stabilization strategy consists in using first-order accurate monotone upwind methods (Donor-Cell, Godunov). This approach is often used but can lead to non-accurate solutions due to excessive numerical diffusion. However the application of these methods to turbulent flows can be improved by a multi-dimensional approach.

A second option consists in using second order upwind total variation diminushing (TVD) methods with limiters. One must notice that TVD methods

are second-order accurate when the mesh is refined enough to represent well the solution details. In practical applications, when limiters are applied, a 50% heavier mesh than with fully second order method (without limiters) can be necessary.
In our study, we choose the last approach for the flow variables.
As far as the solution algorithm is concerned, the main difficulties are related to the flat mesh elements and the non-linear problem stiffness. The choice of a non-structured method carries an extra complexity. Pointwise Gauss-Seidel iterations are used to solve the linear system. For the non-linear stiffness, we examinate various options for the linearization.
The paper is organized as follows :
We first describe the basic high-Reynolds number $k-\varepsilon$ model of Launder and Spalding [3]. Then three efficient low-Reynolds number models, namely those of Lam-Bremhorst [4], Nagano-Tagawa [5] and Speziale-Abid-Anderson [6], are presented. In Section 3, we discuss the problem related to the boundary conditions which can lead to numerical stiffness. In Section 4, we present the numerical implementation which is based on a mixed finite-volume / finite-element formulation on unstructured meshes. In the last section, we apply this numerical method combine to different turbulence models to the subsonic flow in a duct and the supersonic flow on a flat plate.

1 Description of the models

1.1 Governing equations of high-Reynolds number $k-\varepsilon$ models

The governing equations are obtained by Reynolds averaging the compressible Navier-Stokes equations, and modeling the Reynolds stress by the Boussinesq assumption.
These equations can be written in a conservative form as :

$$
\left\{
\begin{array}{l}
\dfrac{\partial \rho}{\partial t} + \dfrac{\partial \rho u}{\partial x} + \dfrac{\partial \rho v}{\partial y} = 0 \\
\dfrac{\partial \rho u}{\partial t} + \dfrac{\partial \rho u^2 + p}{\partial x} + \dfrac{\partial \rho uv}{\partial y} = \dfrac{\partial \tau_{xx}}{\partial x} + \dfrac{\partial \tau_{xy}}{\partial y} + \dfrac{\partial}{\partial x}\left(\tau^t_{xx} - \dfrac{2}{3}\rho k\right) + \dfrac{\partial \tau^t_{xy}}{\partial y} \\
\dfrac{\partial \rho v}{\partial t} + \dfrac{\partial \rho uv}{\partial x} + \dfrac{\partial \rho v^2 + p}{\partial y} = \dfrac{\partial \tau_{xy}}{\partial x} + \dfrac{\partial \tau_{yy}}{\partial y} + \dfrac{\partial \tau^t_{xy}}{\partial x} + \dfrac{\partial}{\partial y}\left(\tau^t_{yy} - \dfrac{2}{3}\rho k\right) \\
\dfrac{\partial E}{\partial t} + \dfrac{\partial u(E+p)}{\partial x} + \dfrac{\partial v(E+p)}{\partial y} = \dfrac{\partial (u\tau_{xx} + v\tau_{xy})}{\partial x} + \dfrac{\partial (u\tau_{xy} + v\tau_{yy})}{\partial y} + \dfrac{\partial}{\partial x}\left(\lambda \dfrac{\partial T}{\partial x}\right) \\
\qquad + \dfrac{\partial}{\partial y}\left(\lambda \dfrac{\partial T}{\partial y}\right) + \dfrac{\partial (u\tau^t_{xx} + v\tau^t_{xy} - \frac{2}{3}\rho k u)}{\partial x} \\
\qquad + \dfrac{\partial (u\tau^t_{xy} + v\tau^t_{yy} - \frac{2}{3}\rho k v)}{\partial y} + \dfrac{\partial}{\partial x}\left(\lambda_t \dfrac{\partial T}{\partial x}\right) + \dfrac{\partial}{\partial y}\left(\lambda_t \dfrac{\partial T}{\partial y}\right) \\
\qquad + \dfrac{\partial}{\partial x}\left(\dfrac{\mu_t}{\sigma_k}\dfrac{\partial k}{\partial x}\right) + \dfrac{\partial}{\partial y}\left(\dfrac{\mu_t}{\sigma_k}\dfrac{\partial k}{\partial y}\right)
\end{array}
\right.
$$

where ρ denotes the fluid density, u and v the x and y component of fluid velocity.
The total energy per unit volume E is defined by :

$$E = \rho C_v T + \frac{1}{2}\rho(u^2 + v^2) + \rho k \ ,$$

where C_v is the specific heat at constant volume, T the temperature and k the turbulent kinetic energy.
The pressure p can be calculated from the equation of state of a perfect gas :

$$p = (\gamma - 1)\rho C_v T$$

In the above equations, λ and λ_t are the laminar and eddy thermal viscosity, and τ and τ_t represents respectively the laminar and turbulent stress tensor

which are given by

$$\tau_{xx} = 2\mu\frac{\partial u}{\partial x} - \frac{2}{3}\mu\left(\frac{\partial u}{\partial x} + \frac{\partial v}{\partial y}\right)$$

$$\tau_{yy} = 2\mu\frac{\partial v}{\partial y} - \frac{2}{3}\mu\left(\frac{\partial u}{\partial x} + \frac{\partial v}{\partial y}\right)$$

$$\tau_{xy} = \tau_{yx} = \mu\left(\frac{\partial u}{\partial y} + \frac{\partial v}{\partial x}\right)$$

$$\tau^t_{xx} = 2\mu_t\frac{\partial u}{\partial x} - \frac{2}{3}\mu_t\left(\frac{\partial u}{\partial x} + \frac{\partial v}{\partial y}\right)$$

$$\tau^t_{yy} = 2\mu_t\frac{\partial v}{\partial y} - \frac{2}{3}\mu_t\left(\frac{\partial u}{\partial x} + \frac{\partial v}{\partial y}\right)$$

$$\tau^t_{xy} = \tau^t_{yx} = \mu_t\left(\frac{\partial u}{\partial y} + \frac{\partial v}{\partial x}\right)$$

where μ is the laminar viscosity and μ_t the turbulent viscosity which is computed by a suitable turbulence model.

The closure of the system is realized by the high-Reynolds number $k-\varepsilon$ turbulence model of Launder-Spalding [3] which can be written as :

$$\begin{cases} \dfrac{\partial \rho k}{\partial t} + \dfrac{\partial \rho u k}{\partial x} + \dfrac{\partial \rho v k}{\partial y} = \dfrac{\partial}{\partial x}\left(\mu\dfrac{\partial k}{\partial x}\right) + \dfrac{\partial}{\partial y}\left(\mu\dfrac{\partial k}{\partial y}\right) + \dfrac{\partial}{\partial x}\left(\dfrac{\mu_t}{\sigma_k}\dfrac{\partial k}{\partial x}\right) + \dfrac{\partial}{\partial y}\left(\dfrac{\mu_t}{\sigma_k}\dfrac{\partial k}{\partial y}\right) \\ \qquad\qquad -\rho\varepsilon + \mathcal{P} \\ \dfrac{\partial \rho \varepsilon}{\partial t} + \dfrac{\partial \rho u \varepsilon}{\partial x} + \dfrac{\partial \rho v \varepsilon}{\partial y} = \dfrac{\partial}{\partial x}\left(\mu\dfrac{\partial \varepsilon}{\partial x}\right) + \dfrac{\partial}{\partial y}\left(\mu\dfrac{\partial \varepsilon}{\partial y}\right) + \dfrac{\partial}{\partial x}\left(\dfrac{\mu_t}{\sigma_\varepsilon}\dfrac{\partial \varepsilon}{\partial x}\right) + \dfrac{\partial}{\partial y}\left(\dfrac{\mu_t}{\sigma_\varepsilon}\dfrac{\partial \varepsilon}{\partial y}\right) \\ \qquad\qquad +c_{\varepsilon_1}\dfrac{\varepsilon}{k}\mathcal{P} - c_{\varepsilon_2}\dfrac{\rho\varepsilon^2}{k} \end{cases}$$

where ε denotes the turbulent dissipation rate and $\mathcal{P}$ the production term of the turbulent kinetic energy which is given by :

$$\mathcal{P} = \mu_t \left(2 \left(\frac{\partial u}{\partial x} \right)^2 - \frac{2}{3} \left(\frac{\partial u}{\partial x} + \frac{\partial v}{\partial y} \right)^2 + \left(\frac{\partial v}{\partial x} + \frac{\partial u}{\partial y} \right)^2 + 2 \left(\frac{\partial v}{\partial y} \right)^2 \right) - \frac{2}{3} \rho k \left(\frac{\partial u}{\partial x} + \frac{\partial v}{\partial y} \right)$$

The eddy viscosity is calculated as :

$$\mu_t = c_\mu \frac{\rho k^2}{\varepsilon}$$

The constants c_μ, σ_k, σ_ε, c_{ε_1} and c_{ε_2} appearing in the above equations are five empirical constants whose values depend on the selected turbulence model. For the model of Launder and Spalding, these values are given by :

$$c_\mu = 0.09,\ \sigma_k = 1.0,\ \sigma_\varepsilon = 1.3,\ c_{\varepsilon_1} = 1.44 \text{ and } c_{\varepsilon_2} = 1.92$$

The high-Reynolds number turbulence equations are used in conjunction with wall functions [19] which give boundary conditions for points situated in the turbulent region (far-wall zones).

1.2 Low-Reynolds number turbulence models modifications

The previous transport equations on k and ε are obtained by assuming that the turbulent effects are dominant in the flow domain [20]. Thus the standard $k-\varepsilon$ model is not valid in regions where the viscous effects are large compared with the turbulent effects (near-wall zones).
In order to account for low-Reynolds number effects (near-wall effects), damping functions f_{ε_1}, f_{ε_2} and f_μ are usually introduced to modify the constants c_{ε_1}, c_{ε_2} and c_μ; these constants are respectively associated to the production term and the dissipation term of ε, and to the eddy viscosity μ_t. Also, extra-terms D and E are sometimes added in the equation of k and ε in order to better represent the near-wall behaviour. These damping functions and extra-terms define the different low-Reynolds number models which can be written in a general form as :

$$\left\{\begin{array}{ll} \dfrac{\partial \rho k}{\partial t}+\dfrac{\partial \rho u k}{\partial x}+\dfrac{\partial \rho v k}{\partial y} & =\dfrac{\partial}{\partial x}\left(\mu\dfrac{\partial k}{\partial x}\right)+\dfrac{\partial}{\partial y}\left(\mu\dfrac{\partial k}{\partial y}\right)+\dfrac{\partial}{\partial x}\left(\dfrac{\mu_t}{\sigma_k}\dfrac{\partial k}{\partial x}\right)+\dfrac{\partial}{\partial y}\left(\dfrac{\mu_t}{\sigma_k}\dfrac{\partial k}{\partial y}\right) \\ & \quad -\rho\varepsilon+\mathcal{P}+\boldsymbol{D} \\ \dfrac{\partial \rho \varepsilon}{\partial t}+\dfrac{\partial \rho u \varepsilon}{\partial x}+\dfrac{\partial \rho v \varepsilon}{\partial y} & =\dfrac{\partial}{\partial x}\left(\mu\dfrac{\partial \varepsilon}{\partial x}\right)+\dfrac{\partial}{\partial y}\left(\mu\dfrac{\partial \varepsilon}{\partial y}\right)+\dfrac{\partial}{\partial x}\left(\dfrac{\mu_t}{\sigma_\varepsilon}\dfrac{\partial \varepsilon}{\partial x}\right)+\dfrac{\partial}{\partial y}\left(\dfrac{\mu_t}{\sigma_\varepsilon}\dfrac{\partial \varepsilon}{\partial y}\right) \\ & \quad +c_{\varepsilon_1}\boldsymbol{f}_{\varepsilon_1}\dfrac{\varepsilon}{k}\mathcal{P}-c_{\varepsilon_2}\boldsymbol{f}_{\varepsilon_2}\dfrac{\rho\varepsilon^2}{k}+\boldsymbol{E} \end{array}\right.$$

where the eddy viscosity is given by :

$$\mu_t = c_\mu \boldsymbol{f}_\mu \frac{\rho k^2}{\varepsilon}$$

Many low-Reynolds number $k-\varepsilon$ models have been proposed and tested [9, 10, 5, 6].
Three of them, which seem to give satisfactory results [9, 11, 7], have been selected in this study, namely the model of Lam-Bremhorst [4] and the more recent improved models of Nagano-Tagawa [5] and Speziale-Abid-Anderson [6]. These models are presented in this section.
The variables R_t, R_y and y^+ appearing in the equations below respectively denote two local Reynolds numbers and a non-dimensional normal distance to the wall. They are given by :

$$R_t = \frac{\rho k^2}{\mu\varepsilon}$$

$$R_y = \frac{\rho\sqrt{k}y}{\mu}$$

$$y^+ = \frac{u_f\, y}{\nu}$$

where ν is the kinetic laminar viscosity ($\nu = \frac{\mu}{\rho}$), and u_f the friction velocity ($u_f = \sqrt{\frac{\tau_\omega}{\rho}}$, τ_ω the shear stress at the wall).

The model of Lam-Bremhorst :

The extra-terms D and E are set to zero and the damping functions are defined by :

$$\begin{cases} f_{\varepsilon_1} = 1 + \left(\frac{0.05}{f_\mu}\right)^3 \\ \\ f_{\varepsilon_2} = 1 - exp\left[-(R_t)^2\right] \\ \\ f_\mu = \left[1 - exp(-0.0165\ R_y)\right]^2 \left(1 + \frac{20.5}{R_t}\right) \end{cases}$$

The empirical constants are given by :
$c_\mu = 0.09$, $\sigma_k = 1.0$, $\sigma_\varepsilon = 1.3$, $c_{\varepsilon_1} = 1.44$ and $c_{\varepsilon_2} = 1.92$

The model of Nagano-Tagawa :

The extra-terms D and E are set to zero and the damping functions are defined by :

$$\begin{cases} f_{\varepsilon_1} = 1. \\ f_{\varepsilon_2} = \left\{1 - 0.3\ exp\left[-\left(\frac{R_t}{6.5}\right)^2\right]\right\}.\left\{1 - exp\left(\frac{-y^+}{6}\right)\right\} \\ f_\mu = \left\{exp\left(\frac{-y^+}{26}\right)\right\}^2.\left\{1 + \frac{4.1}{R_t^{3/4}}\right\} \end{cases}$$

The empirical constants are given by :
$c_\mu = 0.09$, $\sigma_k = 1.$, $\sigma_\varepsilon = 1.3$, $c_{\varepsilon_1} = 1.45$ and $c_{\varepsilon_2} = 1.92$

The model of Speziale-Abid-Anderson :

The extra-terms D and E are set to zero and the damping functions are defined by :

$$\begin{cases} f_{\varepsilon_1} = 1. \\ f_{\varepsilon_2} = \left\{1 - \frac{2}{9}exp\left[-\left(\frac{R_t}{6}\right)^2\right]\right\}.\left\{1 - exp\left(\frac{-y^+}{4.9}\right)\right\}^2 \\ f_\mu = exp\left(1 + \frac{3.45}{\sqrt{R_t}}\right) tanh\left(\frac{y^+}{70}\right) \end{cases}$$

The empirical constants are given by :
$c_\mu = 0.09$, $\sigma_k = 1.36$, $\sigma_\varepsilon = 1.36$, $c_{\varepsilon_1} = 1.44$ and $c_{\varepsilon_2} = 1.83$

One common feature of the previous low-Reynolds number models is that no extra-term is introduced.
One can notice that in regions far away from the wall, the damping functions

become unity so that the high-Reynolds number equations are recovered.
It can also be verified that for the models of Nagano-Tagawa and Speziale-Abid-Anderson the damping functions satisfy $f_1 = O(1)$, $f_2 = O(y^2)$ and $f_\mu = O(1/y)$ near a wall. It follows that these models, contrary to the Lam-Bremhorst model, are asymptotically consistent [6].

2 Boundary conditions

The boundary conditions for the "fluid variables" are the no-slip- and isothermic or adiabatic wall conditions :

$$\begin{aligned}
\left(\frac{\partial \rho}{\partial n}\right)_{y=0} &= 0 \\
u_{|_{y=0}} &= 0 \\
v_{|_{y=0}} &= 0 \\
T_{|_{y=0}} &= T_w \qquad \text{(isothermic wall)} \\
&\text{or} \\
\left(\frac{\partial T}{\partial n}\right)_{y=0} &= 0 \quad \text{(adiabatic wall)}
\end{aligned}$$

The boundary condition for the turbulent kinetic energy is :

$k_{|_{y=0}} = 0$

For the turbulent dissipation rate, different boundary conditions have been used by several authors in a variety of applications of the $k-\varepsilon$ model; these are the following :

- Option 1 (see for example [9, 4]) :

$$\left(\frac{\partial \varepsilon}{\partial y}\right)_{|_{y=0}} = 0$$

This boundary condition is easy to implement but there is no solid theoritical or experimental justification. Therefore, the use of this condition can lead to substantial errors.

- Option 2 (see for example [9, 21]) :

$$\varepsilon_{|_{y=0}} = \nu \left(\frac{\partial^2 k}{\partial y^2} \right)_{|_{y=0}}$$

This boundary condition is obtained from the limit of the k equation at the wall and is consistent with asymptotic computations near a wall, but it can lead to numerical stiffness.

- Option 3 (see for example [9, 22, 23]) :

$$\varepsilon_{|_{y=0}} = 2\nu \left(\frac{\partial \sqrt{k}}{\partial y} \right)^2_{|_{y=0}}$$

This boundary condition is obtained from the asymptotic limit of ε near the wall. As the previous one, this condition is consistent with asymptotic computations but can lead to numerical stiffness.

- Option 4 :
The boundary condition suggested by Chapman and Kuhn [18] :

$$\varepsilon_{|_{y=0}} = \left(4\nu \frac{k}{y^2} - \varepsilon \right)_{y=\delta}$$

where δ is a small distance from the wall.
This last condition, which can be written as

$$\frac{1}{2} \left(\varepsilon_{|_{y=0}} + \varepsilon_{|_{y=\delta}} \right) = \left(2\nu \frac{k}{y^2} \right)_{|_{y=\delta}} ,$$

is an approximation of the previous boundary condition where

$$\left(\frac{\partial \sqrt{k}}{\partial y} \right)_{|_{y=0}} \approx \frac{\sqrt{k}}{\delta} ,$$

and with a mean value of ε evaluated between $y = 0$ and $y = \delta$.

The boundary condition of Chapman and Kuhn is easy to implement and leads to stable results [19]. So, we choose to implement this last condition. The value of δ corresponds to the first mesh increment in the y direction.

3 Numerical implementation

For solving the previous fluid and turbulence equations, a mixed finite element / finite volume formulation is used on unstructured meshes [1]. This numerical method combines an upwind second order (MUSCL) finite-volume approximation for the inviscid terms and a centered finite-element P1-Lagrange approximation for the viscous and source terms (high-Reynolds number versions were derived in [1, 2, 12]). The use of unstructured meshes allows the simulation of flows in complex geometries and the enhancement of the solution accuracy through local mesh refinements.

A Roe approximate Riemann solver is used for the approximation of the fluid convective terms; the positivity-preserving multi-component Riemann flux (Larrouturou's scheme) proposed in [15] is considered for the turbulence convective terms.

The linearized implicit formulation Backward Euler used for time advancing the discrete solution treats in a fully coupled way the flow variables ρ, ρu, ρv, E, on one hand, and the turbulence variables ρk and $\rho\varepsilon$, on the other hand.

For the flow variables, we basically employ the implicit scheme used in [16, 17, 14]. As far as the diffusive terms are concerned, the scheme is based on a classical linearized formulation. In this linearization, we consider the turbulence variables k and ε (and therefore the turbulent viscosity μ_t) as frozen at its value at the previous time level t^n. For the convective terms however, we have to use an approximate linearization since Roe's fluxes are not diffe-

rentiable.
Then, the scheme is written in δ-form as :

$$\left(\frac{Id}{\Delta t} - (\mathcal{F}')^n\right)\left(W^{n+1} - W^n\right) = \mathcal{F}^n \quad ,$$

where Id is the identity matrix and W^n the fluid variables at time level t^n. $\mathcal{F}$ contains the discretized convective and diffusive fluxes and $\mathcal{F}'$ is an approximate Jacobian matrix of $\mathcal{F}$.

In particular, we use a second-order accurate approximation of the convective fluxes for the "explicit part" of the scheme (which provides a second-order accurate steady-state solution if any), and a first-order accurate approximation for the implicit part, which leads to diagonaly-dominant matrices and therefore facilitates the linear system resolution at each time step.

The linear 4×4 block resulting system can be solved by node-Jacobi or node-Gauss-Seidel iterations.

For the integration of the turbulence equations, a similar method is applied. The implicit fluxes are linearized with respect to the variables (ρk) and $(\rho\varepsilon)$, the flow variables being frozen. The scheme is also written in δ-form but in this case $\mathcal{F}_t$ contains a source term in addition to the convective and diffusive fluxes.
Concerning the Jacobian matrix $\mathcal{F}_t'$ of $\mathcal{F}_t$, three options of linearization have been implemented; in all these linearizations, the damping functions and the turbulent viscosity are frozen at their value at the previous time level t^n :

a) The source term is not linearized so that $\mathcal{F}_t'$ contains only the linearized convective and diffusive fluxes.

b) We only linearize the dissipation term of the source term for k and ε, in addition to the linearization of the convective and diffusive fluxes. The production term of k and ε is not linearized in order to obtain a more diagonally-dominant matrix.

We now precise the source term linearization :
Let Ω be the source term defined by :

$$\Omega = \begin{pmatrix} -\rho\varepsilon + \mathcal{P} \\ c_{\varepsilon_1} f_{\varepsilon_1} \dfrac{\varepsilon}{k} \mathcal{P} - c_{\varepsilon_2} f_{\varepsilon_2} \rho \dfrac{\varepsilon^2}{k} \end{pmatrix}$$

where $\mathcal{P}$ denotes the production term of the turbulent kinetic energy.
With this option of linearization, the approximate source term Jacobian relative to the conservative variables ρk and $\rho\varepsilon$ is given by :

$$\Omega' = \begin{pmatrix} 0 & -1 \\ c_{\varepsilon_2} f_{\varepsilon_2} \dfrac{\varepsilon^2}{k^2} & -2c_{\varepsilon_2} f_{\varepsilon_2} \dfrac{\varepsilon}{k} \end{pmatrix}$$

c) The same linearization as in option (b) is done except that the dissipation term $-(\rho\varepsilon)^{n+1}$ of the turbulent kinetic energy becomes $-(\rho\varepsilon)^{n+1} \dfrac{k^{n+1}}{k^n}$. The diagonal dominance of the implicit matrix is then reinforced. With this linearization option, the approximate Jacobian of the source term becomes :

$$\Omega' = \begin{pmatrix} -\dfrac{\varepsilon}{k} & -1 \\ c_{\varepsilon_2} f_{\varepsilon_2} \dfrac{\varepsilon^2}{k^2} & -2c_{\varepsilon_2} f_{\varepsilon_2} \dfrac{\varepsilon}{k} \end{pmatrix}$$

A 1D study [13] has pointed out that the last linearization (option c) is the one that yields the best improvement for the time stability of the scheme.

This linearization of the implicit turbulence terms leads to a 2×2 block linear system that we can solve using the same linear solvers as for the fluid system.

We must also specify that the wall boundary condition of the turbulent dissipation rate ϵ is imposed implicitly to ensure more stability.

As for the flow variables and for the same reason, a second-order accurate approximation of the convective fluxes is used for the explicit part of the scheme and a first-order accurate approximation is applied for the implicit part.

4 Numerical experiments

In the following, y^+, u^+, k^+ and ε^+ denote the non-dimensional values of y, u, k and ε respectively; these are given by :

$$y^+ = \frac{u_f \; y}{\nu}$$
$$u^+ = \frac{u}{u_f}$$
$$k^+ = \frac{k}{{u_f}^2}$$
$$\varepsilon^+ = \frac{\varepsilon \; \nu}{{u_f}^4}$$

where u_f is the friction velocity and ν the kinetic laminar viscosity.

4.1 Comte-Bellot 2D duct

For the validation of our study, we first calculate a 2D flow in a duct. This flow has been experimentally studied by Comte-Bellot [24].
The different experimental parameters used in the simulation are given below :

The half-width of the duct $D = 0.09\ m$;
the kinetic laminar viscosity $\nu = 1.36\ 10^{-5}\ m^2/s$;
the mean velocity at the center of the canal $U = 10.5\ m/s$.

With these values, we obtain the following Reynolds number :

$$Rey = \frac{U.D}{\nu} = 69500$$

Since the solution of this problem is symmetric, the mesh of a half duct with 10×60 points is used (Figure 1). This mesh, a rectangle of 0.9×0.09, is a highly stretched near the wall, smoothly varying mesh. The minimum element length along the y-direction is $3.45\ 10^{-5}$ near the wall. The maximum element

aspect ratio is about 3000.

We first study the effect of the implicit source term linearization on the convergence. Computations are performed with a local time step and a CFL number of 1600 (Courant-Friedrichs-Lewy criterion). For solving the implicit linear systems, we use 20 node-Gauss-Seidel iterations. In Figure 2, we show the convergence obtained with the three linearizations described in Section 4. The model used is Nagano-Tagawa's model (see Section 2), but the same kind of results is obtained with the two other models. We observe that the implicitation which consists in only linearizing the turbulent dissipation terms where the dissipation $-(\rho\varepsilon)^{n+1}$ of the turbulent kinetic energy becomes $-(\rho\varepsilon)^{n+1}\,\dfrac{k^{n+1}}{k^n}$, is the computationally most robust. The time stability is then improved and it allows to use larger time steps to reach the stationary solution.

In Figure 3, the normalized residuals of E and ρk versus the number of time iterations are sketched for the three low-Reynolds number models described in Section 2. We can notice that a faster convergence is obtained with the model of Nagano-Tagawa. Indeed, for this test case this model allows to use larger time steps than those of the two other models. It also turns out that the Lam-Bremhorst's model is the computationally less robust model.

We have then performed computations of the boundary layer with the model of Lam-Bremhorst. We compare the resulting discrete solution with a Lam-Bremhorst's model reference solution obtained by a 1D calculation with 237 (non uniformly distributed) nodes. Indeed, with this particular flow, the general equations system can be simplified to 1D problem. Figure 4 presents a zoom of the u^+, k^+ *and* ε^+ profiles near the wall for both the discrete 2D solution and the reference computations. We can observe a very good agreement between these two solutions.

On Figure 5, we present the profiles of u, k and ε at abscissa $x = 0.9$ (variation of variables in x direction is almost zero). The profiles for the non-dimensional variables u^+, k^+ and ε^+ near the wall are shown on Figure 6. We verify a good agreement between the turbulence models for the behavior of the

model	U_{max}	k^+_{max}/y^+	ε^+_{max}/y^+	ε^+_{wall}	U_f
experimental data	10.5	4.5/20	0.2/10	[0.05;0.1]	0.39
Nagano-Tagawa	9.90	4.24/18	0.18/10.9	0.072	0.397
Lam-Bremhorst	9.91	4.58/18	0.16/8.5	0.045	0.409
Speziale-Abid-Anderson	9.90	4.1/21	0.2/9.3	0.083	0.399

Table 1: Comparison of the discrete solutions (computed with the different turbulence models) with the experimental data.

different quantities in the near- and far-wall region.
We have also verified that $u^+ = y^+$ and $k^+ = O(y^{+2})$ in the viscous sublayer ($y^+ \leq 5$).

Some characteristic values of the discrete solutions are compared with experimental data in Table 1. For each turbulence model, we observe that the calculations give good results. In any case, the relative error is less than $5-6$ %. We notice that except for the maximum of k^+, the model of Lam-Bremhorst gives less accurate results than the two other models.
The computations run on a DEC Alpha 3000 workstation. A residual decrease for ρ, E and k up to 10^{-6} requires about 400 iterations and 9 minutes CPU time when using the model of Nagano-Tagawa for example.

4.2 Mabey supersonic flat plate flow

The second test case is a supersonic boundary layer on an adiabatic flat plate experimentally studied by Mabey [25]. The experiment is performed on a flat plate with a length of 1.65 m. The freestream static pressure, temperature and velocity are given by :

The static pressure $P_e = 3119.30\ Pa$
The temperature $T_e = 61.805\ K$
The streamwise velocity $u_e = 711.97\ m/s$

The normal velocity $v_e = 0\ m/s$

With these values, we obtain a freestream Mach number of 4.5.
The flow Reynolds number of unit length is :

$$Rey/m = 2.82\ 10^7$$

The computational domain is from the first measuring position $x = 0.368\ m$ to the flat plate trailing edge $x = 1.65\ m$. So the plate length is $1.282\ m$. The height of the numerical domain is $0.2\ m$.

The mesh contains 113×81 grid points in the streamwise and normal directions respectively (Figure 7). The mesh spacing is determined by a constant stretching parameter of 1.11 in the normal direction. For the first grid points from the wall, $y^+ = 0.1\ \sim\ 1$. In the streamwise direction, a parabolic distribution is applied with clustering at the leading edge. The maximal ratio between the length of two orthogonal sides of the flattest element is about 4500.

For the inlet boundary conditions, the streamwise velocity and temperature profiles measured at $x = 0.368\ m$ are imposed. The static pressure is $3119.30\ Pa$ and the normal velocity $0\ m/s$.

Because of k and ε inlet profiles well suited to Lam-Bremhorst's model, this one has been chosen for the calculations.

The flow in a compressible boundary layer is characterized by large changes of density and temperature which influence the physical properties as the laminar viscosity μ. To take the variation of μ with temperature into account, the Sutherland's law is used :

$$\mu(T) = \mu_e \frac{T}{T_e} \qquad \text{if } T \leq 120\ K$$

$$\mu(T) = \mu(120) \left(\frac{T}{120}\right)^{1.5} \left(\frac{120 + 110}{T + 110}\right) \qquad \text{if } T \geq 120\ K$$

where μ_e is obtained from the Reynolds number :

$$Rey/m = \frac{\rho_e u_e}{\mu_e}$$

with ρ_e and u_e the freestream values of the density ρ and the streamwise velocity u.

Concerning the effect of the source term linearization on the scheme stability, the same results as for the previous test case are observed. The third linearization proposed in Section 4 leads to the computationaly most robust method. For this difficult test case, computations are performed with a local time step and a CFL number of 10. The normalized residual of the density ρ, the total energy per unit volume E and the turbulent kinetic energy k is plotted in Figure 8. When a first order accurate approximation is applied for the convective flux of k and ε, a CFL number of 20 can be used. For the two other linearizations (a) and (b), we observe numerical unstabilities for CFL number greater than 4.

Figures 9, 10, 11 and 12 show the resulting distribution of the velocity at streamwise locations $x = 0.623,\ 0.876,\ 1.130$ and $1.384\ m$. A rather good agreement between computational results and experimental data is observed.

The resulting x-momentum and Mach number distribution are sketched in Figures 13 and 14. The experimental data of Mabey are not well predicted. This can be explained by the fact that in this experiment, the Mach number is high enough to induce important compressibility effects which are not taken into account by classical $k-\epsilon$ models. Therefore compressibilty terms have to be included to improve these turbulence models [26, 27, 28] as implemented by Yudiana-Buffat [29].

The computed skin friction C_f is plotted in Figure 17, versus the experimental data. We observe a large increase of C_f at the entrance due to the inlet profiles, which leads to higher predicted values along the wall.

At last, the resulting distributions of k^+ and ε^+ are shown in Figures 15 and 16. The well known peaks of k^+ and ε^+ are observed, and a non-zero value of ε^+ at the wall is obtained.

A residual decrease for ρ, E and k up to 10^{-4} requires about 4200 iterations and 11.5 hours CPU time on a DEC Alpha 3000 workstation.

Conclusion

In this paper, an implicit method based on a linearized formulation has been proposed for the calculation of turbulent boundary layers.

The linearized implicit scheme treats in a decoupled way the flow variables and the turbulence variables but takes into account in a positivity-preserving manner the turbulence variables.

This method has been first applied to a simple test case with three different low-Reynolds $k - \varepsilon$ turbulence models. For these computations, a local time step and CFL numbers greater than 1000 have been used.

As a second test case, a supersonic boundary layer has been computed with the turbulence model of Lam-Bremhorst. For this more difficult simulation, a local time step and a CFL number of only 10 have been used.

In the two test cases, cell aspect ratio are more than 3000 and a good accuracy has even been observed.

These 2D calculations do not require prohibitive CPU time and can run on a workstation.

To improve the implicitation, future works must be done to couple in a stronger way the flow variables and the turbulent variables.

Acknowledgements

The author would like to thank G. Carre, D. Guezengar and A. Dervieux from INRIA Sophia-Antipolis for their valuable advices and suggestions.

The author would also like to acknowledge I. Yudiana and C. Le Ribault from ECL Lyon for the fruitful discussions he had with them.

References

[1] OLIVIER C. and LARROUTUROU B., "On the numerical approximation of the k-ε turbulence model for two dimensional compressible flows", *Rapport de recherche INRIA*, N^o 1526, Septembre 1991.

[2] OLIVIER C., "Simulation numérique d'écoulements visqueux compressibles laminaires et turbulents", Thèse, Université de Nice Sophia-Antipolis, 1991.

[3] LAUNDER B.E. and SPALDING D.B., "The Numerical Computation of Turbulent Flows", *Computer Methods in Applied Mechanics and Engineering*, Vol.3, pp. 269-289, 1974.

[4] LAM C.G.K. and BREMHORST K., "A modified form of the $k-\varepsilon$ model for predicting wall turbulence",*Journal of Fluids Engineering*, Vol. 103, 456-460, 1981.

[5] NAGANO Y. and TAGAWA M., "An improved $k-\varepsilon$ model for boundary layer flows", *Journal of Fluids Engineering*, Vol.112, 33-39, March 1990.

[6] SPEZIALE C.G., ABID R. and ANDERSON E.C., "A critical evaluation of two-equations models for near wall turbulence", Icase Report No 90-46, NASA CR 182068, June 1990.

[7] MAVRIPLIS D.J. and MARTINELLI L., "Mutigrid solution of compressible turbulent flow on unstructured meshes using a two-equation model", Icase Report No 91-11, NASA CR 187513, January 1991.

[8] MINER E.W., SWEAN T.S., ROBERT Jr., HANDLER A., LEIGHTON R.I., "Evaluation of wall-damping models by comparison with direct simulations of turbulent channel flow", *VII Th. Intern. Conferences on Numerical Methods in Laminar and Turbulent Flows*, Stanford U.S.A., 1991.

[9] PATEL C., RODI W. and SCHEWERER G., "Turbulence models for near-wall and low-Reynolds-number flows: a review", *AIAA J.*,23,1308-1319, 1985.

[10] MYONG H.K. and KASAGI N., "A New Approach to the Improvement of $k-\varepsilon$ Turbulence Model for Wall-Bounded Shear Flows", *JSME International Journal*, Vol. 33, pp. 63-72, 1990.

[11] PASCAL H.,"Développement d'une méthode Eléments Spectraux pour la simulation d'écoulements turbulents. Application aux modèles de turbulence de proche paroi", *Rapport de stage*, Laboratoire de Mécanique et d'acoustique, Ecole Centrale de LYON, Septembre 1992.

[12] LE RIBAULT C.,"Simulation des écoulements turbulents compressibles par une méthode mixte éléments finis-volumes finis", Thèse, Ecole Centrale de Lyon, 1991.

[13] FRANCESCATTO J.,"Modèles numériques pour les écoulements turbulents transsoniques", *Rapport de stage*, INRIA Sophia-Antipolis, Juin 1994.

[14] STEVE H., "Méthodes implicites efficaces pour la résolution des équations d'Euler en éléments finis", *Rapport de recherche INRIA*, N^o 779, 1987.

[15] LARROUTUROU B., "How to preserve the mass fraction positivity when computing compressible multi-component flows", *Rapport de recherche INRIA*, N^o 1080, 1989.

[16] FEZOUI L., LANTERI S., LARROUTUROU B., OLIVIER C., "Résolution numérique des équations de Navier-Stokes pour un fluide compressible en maillage triangulaire", *Rapport de recherche INRIA*, N^o 1033, 1989.

[17] FEZOUI L., STOUFFLET B., "A class of implicit upwind schemes for Euler simulations with unstructured meshes", *Rapport de recherche INRIA*, N^o 517, 1986.

[18] CHAPMAN D.R. and KUHN G.D., "Navier-Stokes computations of viscous sublayer flow and the limiting behaviour of turbulence near a wall", *AIAA 7th Computational Fluid Dynamics Conf. Cincinatti*, OH, *AIAA*, New-York, 1985

[19] JAEGER M. and DHATT D., "An extended $k-\varepsilon$ finite element model", *International Journal For Numerical Methods In Fluids*, Vol. 14, 1325-1345, 1992.

[20] JONES W.P. and LAUNDER B.E., "The prediction of laminarization with a two-equation model of turbulence", *Int. J. Heat Mass Transfer*, 15, 301-314, 1972.

[21] REYNOLDS W.C., "Computation of Turbulent Flows", *Annual Review of Fluid Mechanics*, Vol. 8, 1976, pp. 183-208.

[22] DUTOYA D. and MICHARD P., "A Program for Calculating Boundary Layers along Compressor and Turbine Blades", *Numerical Methods in Heat Transfer*, edited by R.W. Lewis, K. Morgan, and O.C. Zienkiewicz, John Wiley & Sons, New-York, 1981.

[23] LAUNDER B.E. and SHARMA B.I., "Application of the Energy-Dissipation Model of Turbulence to the Calculation of Flow Near a Spinning Disc", *Letters in Heat and Mass Transfer*, Vol. 1, 1974, pp. 131-138.

[24] COMTE-BELLOT G., "Contribution à l'étude de la turbulence de conduite", Thèse de Docteur ès Sciences, Université de Grenoble, 1963.

[25] FERNHOLZ H.H. and FINLEY P.J., "A critical compilation of compressible turbulent boundary layer data", *AGARDograph*, N^o 223, 1977.

[26] SARKAR S., ERLEBACHER G. and HUSSAINI M.Y., "Compressible homogeneous shear: simulation and modeling", In *Eight Symposium on turbulent shear flows*, Munich sept. 9-11, 1991.

[27] WILCOX D.C., "Turbulence modeling for CFD", *Griffin Printing*, Glendale California, 1993.

[28] ZEMAN O., "Dilatational dissipation: the concept and application in modeling compressible mixing layers", *Physics of Fluids*, pages 178-188, 1990.

[29] YUDIANA I. and BUFFAT M., Test Case TC3.4, Supersonic Boundary Layer, Contribution to the ETMA workshop, Manchester, 1994.

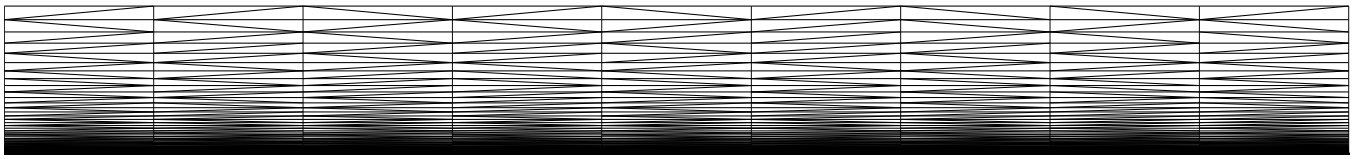

Figure 1: Mesh of the half duct: 10×60 points. 0.09.

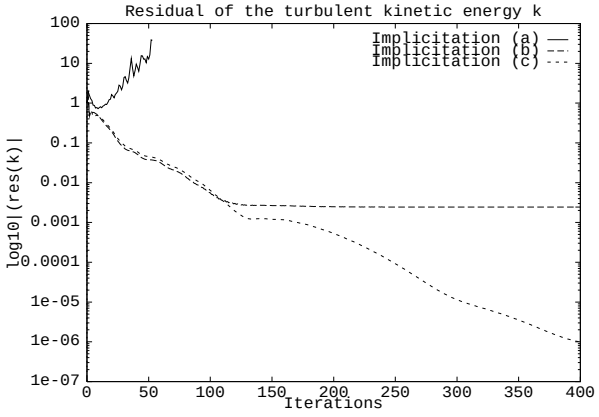

Figure 2: Influence of the implicitation on the convergence. Implicitation (a): the source term is not linearized. Implicitation (b): linearization of the dissipation term of k and ε. Implicitation (c): same linearization as (b) except that the dissipation term $-(\rho\varepsilon)^{n+1}$ becomes $-(\rho\varepsilon)^{n+1}\dfrac{k^{n+1}}{k^n}$.

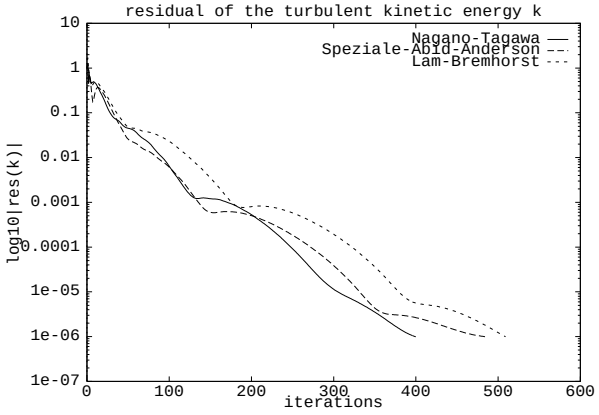

Figure 3: Optimal convergence obtained with the different turbulence models.

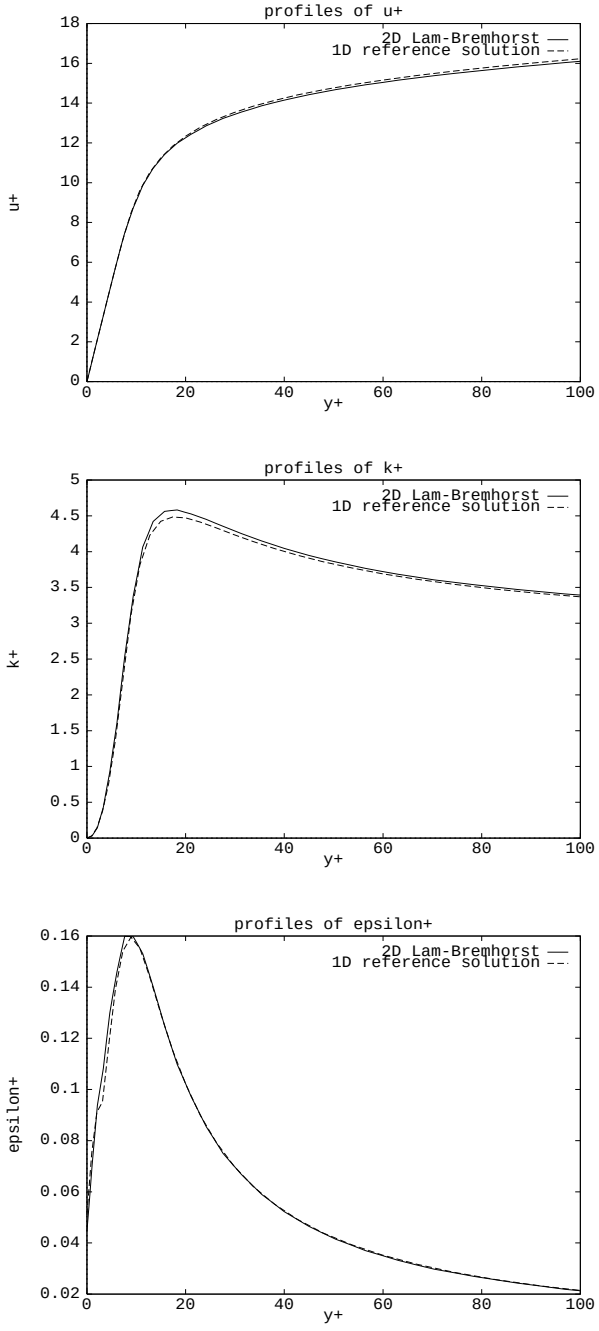

Figure 4: Non-dimensional velocity, turbulent energy and turbulent dissipation comparison with the reference solution near the wall.

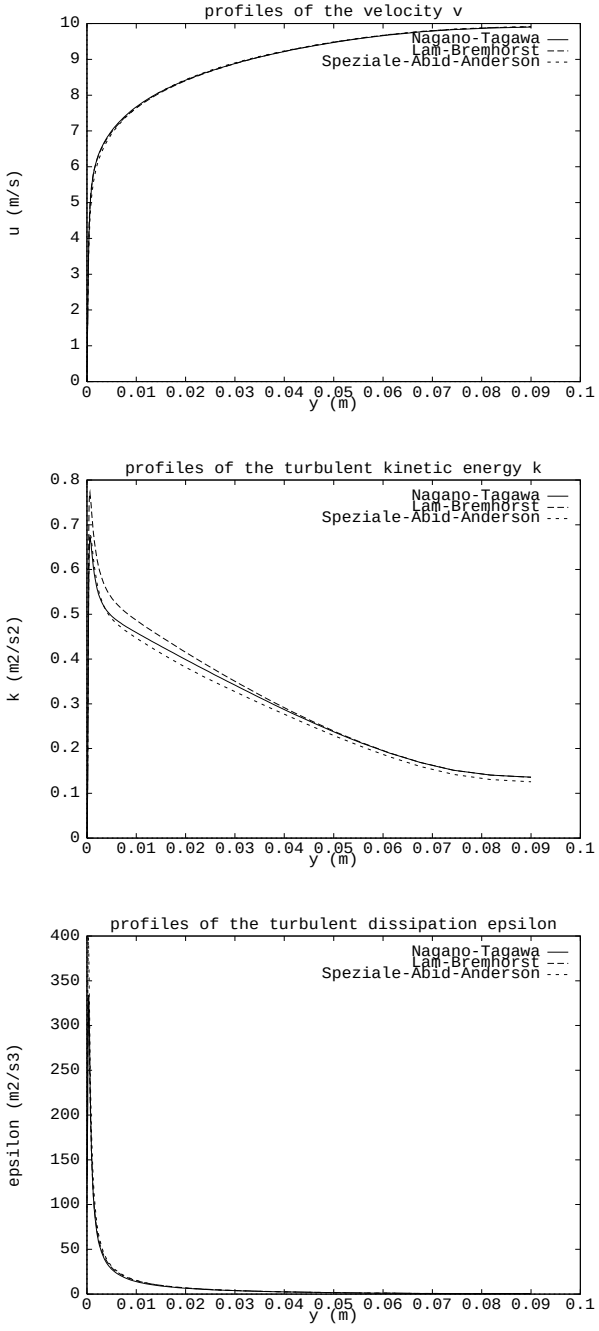

Figure 5: Velocity, turbulent energy and turbulent dissipation for each turbulence model.

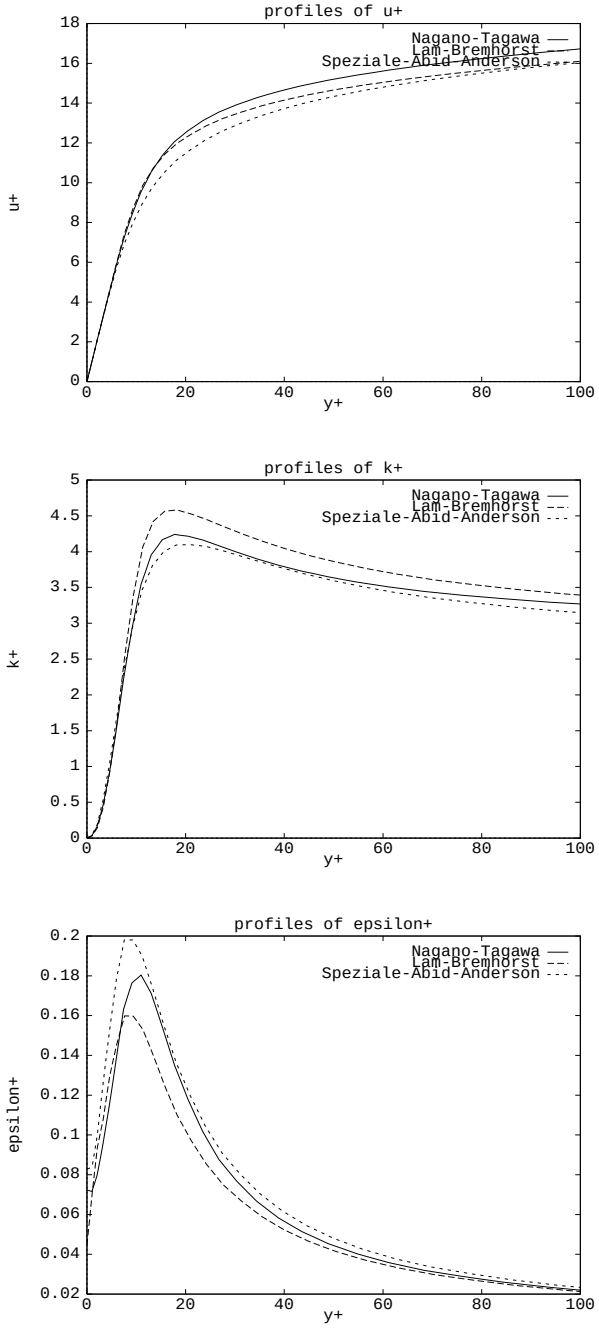

Figure 6: Non-dimensional velocity, turbulent energy and turbulent dissipation near the wall for each model.

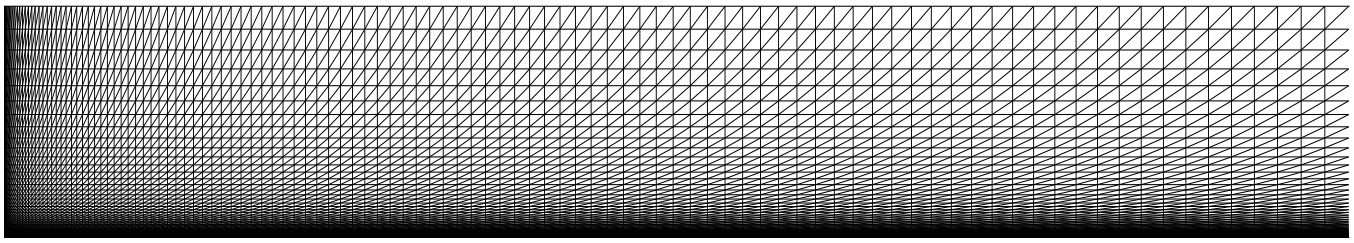

Figure 7: Mesh of the flat plate : 113 × 81 points.

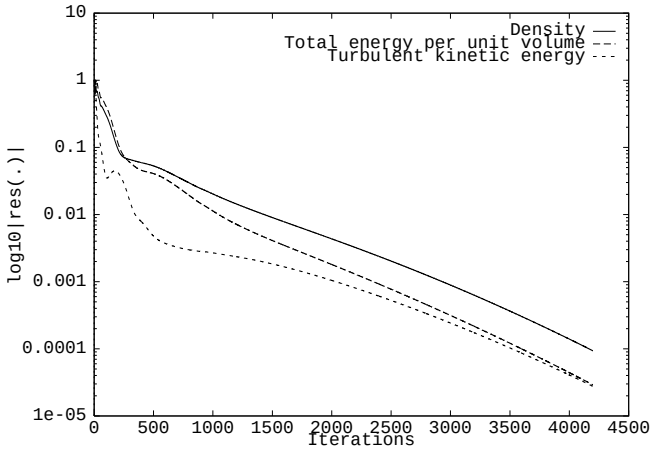

Figure 8: Residual of the density ρ, the total energy E and the turbulent kinetic energy k.

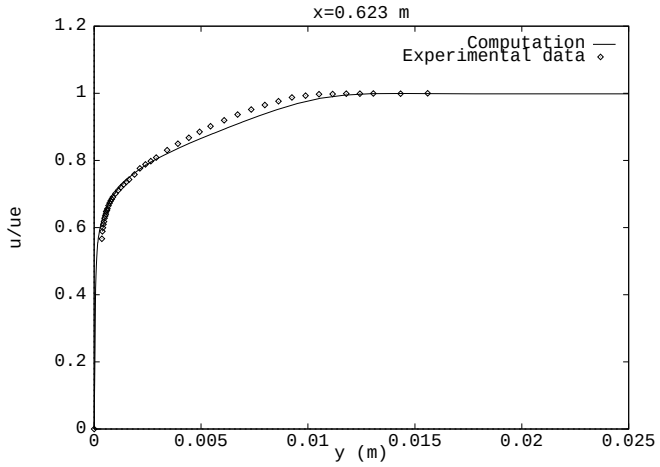

Figure 9: Velocity distribution at streamwise location x=0.623 m

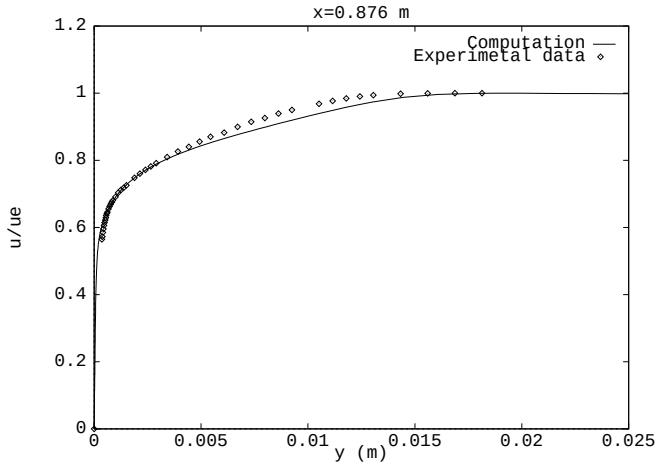

Figure 10: Velocity distribution at streamwise location x=0.876 m

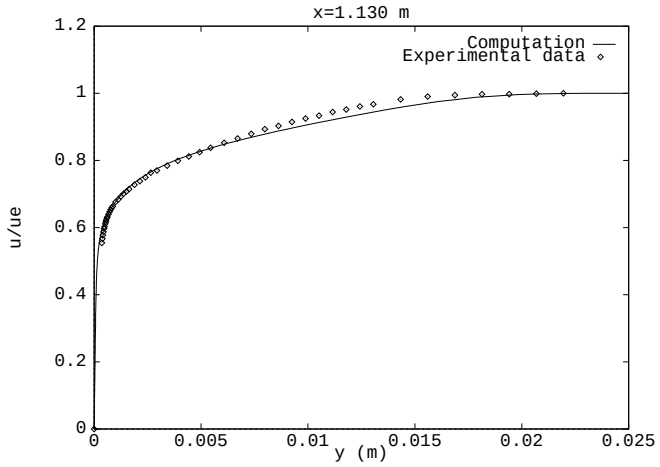

Figure 11: Velocity distribution at streamwise location x=1.130 m

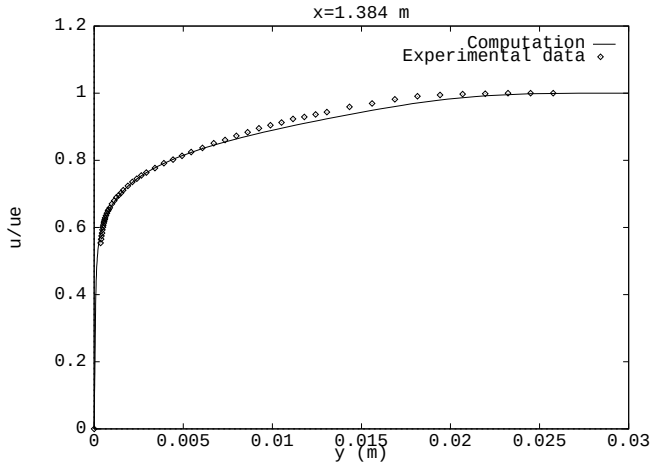

Figure 12: Velocity distribution at streamwise location x=1.384 m

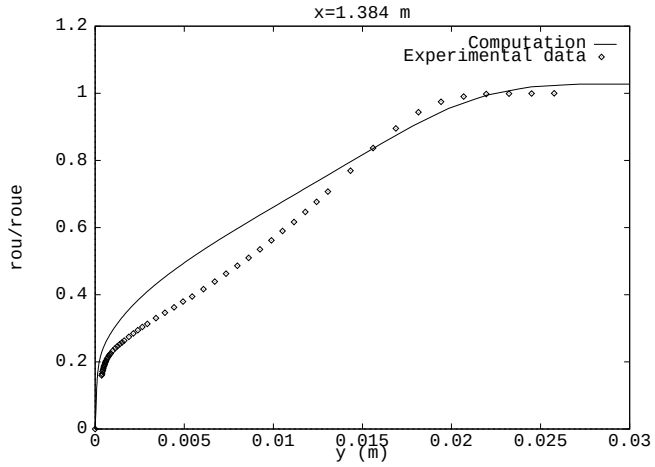

Figure 13: x-momentum distribution at streamwise location x=1.384 m

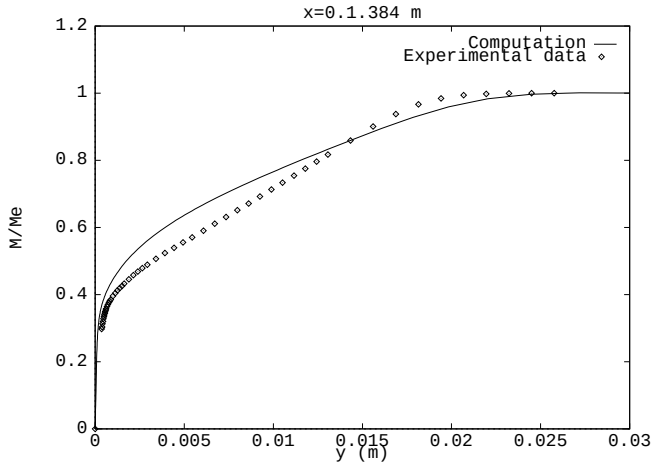

Figure 14: Mach number distribution at streamwise location x=1.384 m

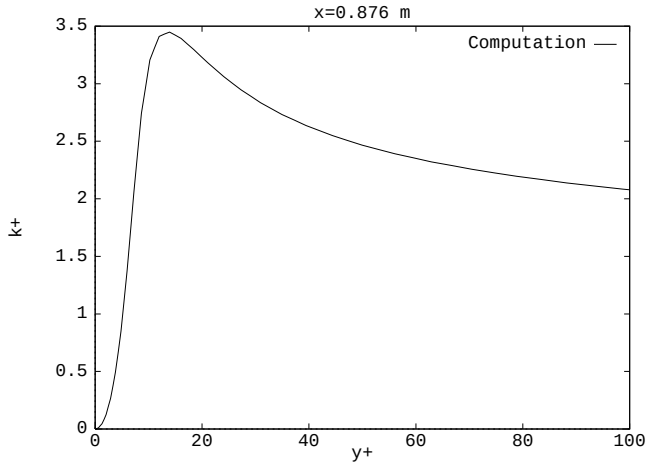

Figure 15: k^+ distribution at streamwise location x=0.876 m

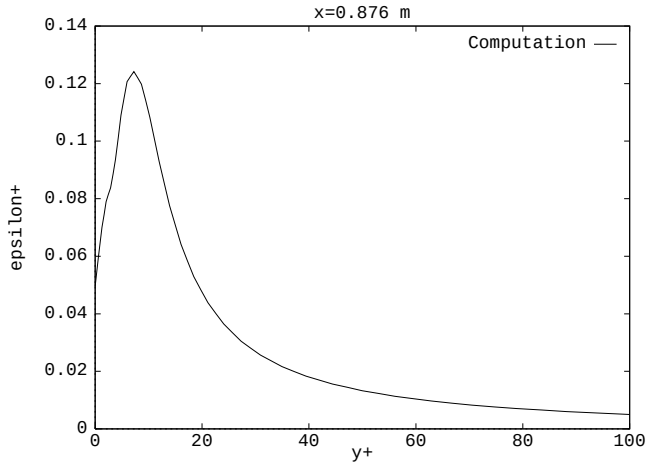

Figure 16: ε^+ distribution at streamwise location x=0.876 m

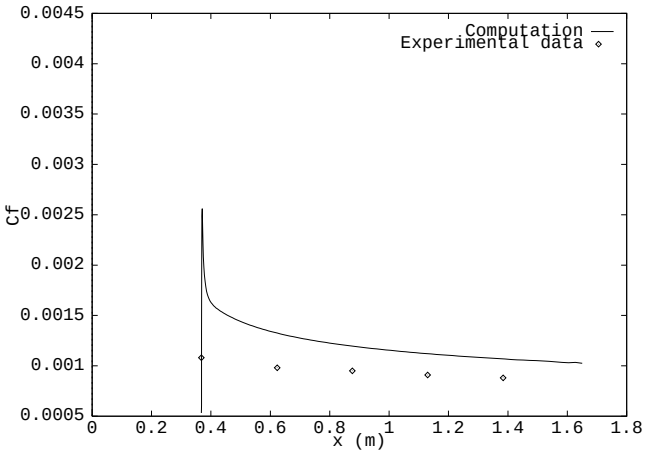

Figure 17: Skin friction distribution, comparison with experimental data.

Unité de recherche INRIA Lorraine, Technopôle de Nancy-Brabois, Campus scientifique,
615 rue du Jardin Botanique, BP 101, 54600 VILLERS LÈS NANCY
Unité de recherche INRIA Rennes, Irisa, Campus universitaire de Beaulieu, 35042 RENNES Cedex
Unité de recherche INRIA Rhône-Alpes, 46 avenue Félix Viallet, 38031 GRENOBLE Cedex 1
Unité de recherche INRIA Rocquencourt, Domaine de Voluceau, Rocquencourt, BP 105, 78153 LE CHESNAY Cedex
Unité de recherche INRIA Sophia-Antipolis, 2004 route des Lucioles, BP 93, 06902 SOPHIA-ANTIPOLIS Cedex

Éditeur
INRIA, Domaine de Voluceau, Rocquencourt, BP 105, 78153 LE CHESNAY Cedex (France)
ISSN 0249-6399